Version: 4th July 2020

Article Body Template

Functional characterization of HIC, a P2Y1 agonist, as a p53 stabilizer for prostate cancer cell death induction

Originally published in Future Medicinal Chemistry 2021, 13:21

ABSTRACT

Graphical abstract available: https://doi.org/10.4155/fmc-2021-0159

Background: 1-(2-hydroxy-5-nitrophenyl)(4-hydroxyphenyl)methyl)indoline-4-carbonitrile (HIC), an agonist of $P2Y_1$ receptor ($P2Y_1R$), induces cell death in prostate cancer (PCa) cell. However, the molecular mechanism behind the inhibition of HIC in PCa remains elusive. **Methods and results:** Here, to outline the inhibitory role of HIC on PCa cells, PC-3 and DU145 were treated with the respective IC_{50} concentrations, which reduced the cell proliferation, adherence property and spheroid formation. HIC was able to arrest the cell cycle at G1/S phase, and also induces apoptosis and DNA damage validated by gene expression profiling. HIC inhibited the PCa cells migration and invasion, revealed its anti-metastatic ability. P2Y1R targeted HIC affects p53, mitogen-activated protein kinase (MAPK), and nuclear factor kappa-light-chain B (NF-κB) protein expression, thereby improves the p53 stabilization essential for the G1/S arrest and cell death. **Conclusion:** These findings provide an insight on the potential use of HIC that remained the mainstay treatment for the prostate cancer.

Keywords: Prostate cancer, P2Y1 receptor, signaling pathways, apoptosis, cell death.

Version: 4th July 2020

Article Body Template

Article Body Template

1. INTRODUCTION

Prostate cancer (PCa) is the second leading cause of death in males, worldwide [1,2] but the molecular mechanism behind the PCa cell invasion and migration is very limited [2]. This has allowed the development of novel therapies with specific targets. G-protein coupled receptor (GPCR), is a plasma membrane receptor whose signaling regulates plethora of biological functions in tumorigenesis [3]. GPCR when overexpressed by the circulating agonist can contribute to the tumor cell growth. Thus, GPCRs targeted drugs are considered as a promising therapeutic strategy for treating a variety of cancers, namely PCa [4]. At least one-third of all marketable drugs are GPCR based agonists or antagonists [3,4] of which only a few are successfully exploited to inhibit cancer signaling pathways. Among GPCRs, purinergic receptors 1 ($P2Y_1R$) are highly expressed in PC3 and DU145 cells in cancer cells [5–8]. $P2Y_1R$ is also suggested as a therapeutic target for suppressing PCa cell growth [6,9]. The activity of $P2Y_1R$ has been investigated in the different biological responses such as cell death and proliferation [9–11]. Signaling pathways regulated by $P2Y_1R$ are dependent on cellular context. For example, the activation of $P2Y_1R$ in Madin-Darby canine kidney epithelial cells (MDKC) and lymphatic endothelial cells strongly promote cell growth by inducing intracellular calcium (Ca^{2+}) level [10,12]. On the other hand, the activation of $P2Y_1R$ is known to induce apoptosis and suppress the cell proliferation in other cell types [9,13]. $P2Y_1R$-Gq protein is linked to phospholipase C (PLC) activation that plays a crucial role in the transmission of astrocytic Ca^{2+} levels, inositol-trisphosphate (IP3), and the activation of protein kinase C (PKC) [14,15]. It is known that

activation of PKC isoform by $P2Y_1R$ can stimulate the extracellular signaling kinase (ERK)- a member of the mitogen-activated protein kinase (MAPK) [16,17]. MAPK signal transduction pathway is also associated with cell proliferation and differentiation [18]. ERK1/2 is known to increase p53 stabilization, required for G1 arrest in ZL55 cell cycle [19].

Several agonists- or antagonists-like compounds of $P2Y_1R$ have been considered as potential cancer therapeutics drugs [13,20,21]. For example, MRS 2365, a selective agonist of P2Y1R, inhibits cell growth and induces cell apoptosis and caspase 3 activity of PC3 cells [6]. Furthermore, 2-methilthioadenosine diphosphate (2-MeSADP) and ADP, non-selective agonists of $P2Y_1R$, induce intracellular transduction pathways involving intracellular Ca^{2+}, PKC, phosphorylation of ERK1/2, and JNK1/2 in ZL55 cell [19]. Thus, ADP promotes $P2Y_1R$ activation, p53 stabilization-mediated G1 cell arrest, and inhibits mesothelioma progression [19]. On other side, MRS2179, as an antagonist of $P2Y_1R$, leads to phosphorylate ERK1/2 and contributes to the re-endothelialization after vascular injury [22]. Thus, focusing on the appropriate downstream signaling pathway of P2Y1R is considered as an important therapeutic target against PCa.

Earlier it was identified that 1-(2-hydroxy-5-nitrophenyl)(4-hydroxypheyl)methyl)indoline-4-carbonitrile (HIC) (Figure 1), a synthesized agonist of $P2Y_1R$, induced cell death and apoptosis in PCa model [9]. Also, HIC was found to induce the capase3/7 activity and reactive oxygen species (ROS) formation and thus inhibited the cell proliferation in the long-term treatment [9]. The anti-cancer effect of HIC was also observed through the analysis of apoptosis [9]. Although the activity of HIC in relation to $P2Y_1R$ activity was identified, the detailed mechanism in PCa cells remains

elusive. Therefore, the present study was aimed at evaluating and exploring the anti-cancer effect of HIC on PC3 and DU145 cells. Colony assay and spheroid assays were performed to determine the anti-cancer effect of HIC on PCa cells. High-throughput sequencing analysis was also performed to identify the regulated genes at the transcription levels in cell cycle arrest and apoptosis pathway. Further, the anti-metastasis effect of HIC was evaluated by wound-healing, migration, and invasion assay. Differential expression of protein involved in MAPK and NF-κB pathway was identified through protein array analysis to elucidate the role of HIC through $P2Y_1R$ activation in PCa cells. Thus, it has been identified that HIC could inhibit cell proliferation and migration through the modulation of MAPKs and p53 signaling pathways.

2. EXPERIMENTAL SECTION

2.1. Chemical synthesis

HIC was designed and synthesized as previously described [9]. Briefly, HIC was synthesized after adding indoline-4-carbonitrile to 2-hydroxy-5-nitrobenzaldehyde and (4-hydroxyphenyl) boronic acid in 5.0 mL DCE and 0.5 mL ethanol at 50°C. After stirring for 70 min at that temperature, solvents were evaporated under reduced pressure and the residue purified through gradient column chromatography. The compound was solubilized to a 100 mM stock solution in dimethyl sulfoxide (DMSO; Sigma-Aldrich, St. Louis, MO, USA).

2.2. Cell culture

PC3 and DU145 cells were cultured in Minimum essential medium eagle at 37°C (MEME, cat no. 4655; Sigma-Aldrich) containing 10% (v/v) fetal bovine serum (FBS, cat no. S181H; Biowest, France), 50 U/mL penicillin, and 50 u/ml streptomycin (Sigma-Aldrich). PCa cells were maintained at 37°C in a humidified incubator with 5% CO_2 and the cells were passaged using 1X Trypsin solution (Cat no. 59427C; Sigma-Aldrich) for every 3 – 5 days. All the experiments were performed in triplicates and the cells were counted using Trypan blue staining (Cat no. T8154; Sigma-Aldrich) inTC-10 automated cell counter (Bio-Rad, Hercules, CA).

2.3. Colony assay

The colony assay was performed using the method previously reported by [23]. Briefly, the non-transfected cells and transfected cells were seeded in 6-well culture plates at the density of 1.0 × 10^3 cell per well. After 24 h, the cells were treated with DMSO, HIC, and MRS 2365. The cells were maintained in an appropriate cell culture environment and the fresh medium was changed for every 4 days and the cells were retreated with HIC after each medium change. After 9 days of post treatment, colonies formed were washed with Phosphate buffered saline (PBS), fixed with 75% methanol (MeOH) and 25 % acid acetic for 10 min. The plates were then stained with 0.5%

crystal violet in ethanol (EtOH) for 15 min. Colonies were counted using an Axiovert 200 M microscope (Carl Zeiss, Germany). Survival fraction was calculated using the following equation.

$$Inhibitory\ ratio\ (\%) = \frac{No.of\ colonies\ treated\ with\ drugs}{No.of\ cell\ treated\ with\ vehicle} \times 100\% \text{ ------- Eq. (1)}$$

To investigate the anti-cancer effect of HIC on PC3 and DU145 cells, cells were plated in 12-well culture plates with the density of 1×10^5 cells/well. After 24 h, the cells were treated with DMSO and / or HIC at the IC_{50} concentration (15.98 µM for PC3 cells and 15.64 µM for DU145 cells). The cells were incubated for 48 h and then washed with warm PBS (pH 7.2) to remove the floating death cells. Images was captured using a Nikon TE 2000-U microscope (Nikon Inc., Japan) at 20x magnification with scale bar = 100 µm.

2.4. Matrix preparation

Corning® Matrigel® Basement Membrane Matrix (Cat no. 354234; Corning, NY, USA) was used for coating the culture plates as the datasheet. A matrigel bottle was thawed and aliquoted to 500 µl and stored at -20°C until use. For invasion assay, 1% matrigel stock solution was prepared using RHB-A medium (Y40001, AH diagnostics, Finland). The working solution was used to sufficiently cover the well surface for Spheroids assay. The Matrigel was kept in the incubator for 2 h.

2.5. MTS invasion assay

PC3 and DU145 cells were seeded in 12 well plates at a density of 1×10^3 cells per well for 48 h. The plates were added with 0.1% Matrigel after the removal of media and subjected to overnight incubation. The spheroids were treated with 5 µM, 10 µM, and 20 µM of HIC for 8 days. The spheroid formation was captured using a Nikon TE 2000-U microscope at 40x magnification. Spheroid area was measured using ImageJ software 1.52 (National Institutes of Health, USA).

To determine the anticancer effect of HIC in the spheroid development in a time dependent manner, colonospheres were treated with the IC_{50} concentration of HIC, 1µM MRS2365 and DMSO as the control. The effect was analyzed for varying period such as day 1, day 3 and day 8. The images of Spheroid formation were captured at the different time point. Spheroid area was quantified using ImageJ software version 1.52 using the equation given below. All data shown were calculated as mean ± SEM, *n = 6*, scale bar = 100 µm (magnification = 40×).

$$\text{Sphere area } \% = \frac{\text{Spheroid area of samples treated drug}}{\text{Spheroid area of control groups}} \times 100\% \text{ ------- Eq. (2)}$$

2.6. mRNA extraction

PC3 and DU145 cells were seeded in the 6-well plates with the density of 5×10^5 cells/well. After overnight incubation, cells were treated with IC_{50} concentration of HIC and DMSO as a control at 37°C for 48 h. The cells were collected by centrifugation and total mRNA was collected using GeneJET RNA Purification kit (cat no. K0731; Thermo Scientific) following the manufacturer's

protocol. Briefly, cells were extracted in lysis buffer supplemented with 400 mM β-mercaptoethanol (Cat no. M6250, Sigma-Aldrich). The lysates were centrifuged at 10,000 rpm for 10 min. The supernatants were transferred into a new RNase-free microcentrifuge tube. EtOH (96-100%) was added and mixed gently by pipetting. Lysates were transferred to the purification column inserted in the collection tube and washed twice with wash buffer. Purified RNA was dissolved in nuclease -free water. The concentration of mRNA was measured using Magellan™ microplate reader (Tecan Group Ltd., Switzerland).

2.6. Illumina sequencing and bioinformatics analysis

The twelve RNA samples extracted were transferred to Biomedicum Functional Genomics Unit (FuGU, University of Helsinki, Helsinki, Finland) for whole transcriptome sequencing using Illumina NextSeq 500 [24]. The bcl data from the RNAseqquencing was converted into FASTQ file format for further insilico analysis.

2.7. RNASeq data analysis

The Human genome FASTA file and gene annotation GTF file were obtained from Ensembl [25] based on FasQC [26]. STAR, Spliced Transcripts Alignment to a Reference, an open-source aligner, was used to calculate read counts, detected the differential level of genes, and map read to the human genome [27]. Differential expression analysis was determined by SAMtools [28] and the

"union" mode of HTSeq [29] using the high-performance research computing resources provided by TUT TCSC Narvi Cluster (*https://wiki.eduuni.fi/display/tutsqn/TUT+Narvi+Cluster*). Differential gene expressions (DEG) with a q-value less than 0.05 weas identified using DESeq2 [30] using R programming. The p-values were adjusted for multiple testing using the Benjamini-Hochberg procedure [31]. A false discovery rate adjusted p-value (i.e., q-value) < 0.05 was set for the selection of DEG genes.

2.8. Gene ontology (GO) and pathway analysis

The combination of Gene ontology and the ClusterProfiler package was used for pathway analyses [32,33]. We performed GO biological process and Kyoto encyclopedia of genes and genomes (KEGG) pathways over-representation test using the gene signature obtained from the DEGs analysis [34]. The packages support the analysis of human genome. For multiple testing and correction, the combination of binomial test, Bonferroni correction, and z-scores was created using the standard to check the regulated genes either inhibited or activated by HIC. In both the KEGG pathways and GO terms, the statistical analyses were used with a cut-off p-value < 0.05.

2.9. Annexin V-FITC apoptosis assay

To detect the effect of HIC on apoptosis, PC3 and DU145 cells were subjected to Annexin V-FITC apoptosis detection kit (Cat no. APOAF-20TST, Sigma-Aldrich). PCa cells were plated in 6-well culture plate with the density of 2×10^5 cells/well. Cells were treated with DMSO (vehicle control) and / or 16 µM HIC for 48 h in the incubator. Cells were then washed with PBS and resuspended with the binding buffer and incubated for 15 min in the dark, according to the manufacturer's protocols. After adding additional binding buffer, cells were detected under an epifluorescence microscope (Nikon-Eclipse Ti-E inverted fluorescence microscope) using 20× objective.

2.10. Cell cycle assay

The drug intervention at different cell cycle phase was identified by propidium iodide kit (Sigma-Aldrich, Cat no. P4170) following manufacturer protocol. Briefly, PC3 and DU145 cells were plated in 6-well plates at the density of 3×10^5 cells/well and incubated overnight. PCa cells were incubated with DMSO, MRS2365, and HIC for 48 h. Then, the cells were collected and resuspended in cold PBS. Subsequently, cells were fixed with cold 70% ethanol and then incubated on ice for 30 min. The pellets were collected by centrifugation and resuspended in PI-Triton-RNase including propidium iodide, Triton X-100, and RNaseA for 15 min in the dark condition. Images were captured using EVOS FL at 40x magnification. Around 300 cells of each condition were observed under the microscope. The photos were analyzed using CellProfiler 4.0 and the cell cycle phases were analyzed using MATLAB R2018b (MathWorks Ltd., MA, USA).

2.11. Wound-healing assay

PC3 and DU145 cells were seeded in 6-well plates at a density of 1.5 × 10^6 cells/well and maintained until 90% confluence was reached. The plates were carefully scratched using 200 µl pipette tips to draw a linear "wound" in the cell monolayer of each well. The plates were washed 2 times with warm PBS to remove the floating cells and incubated in MEME media containing 1% FBS in the presence and absence of HIC or MRS2365 for 24 h. The control well was added with 0.1% DMSO as the vehicle control. The images of the migrated cells into the wound surface were captured using a Nikon TE 2000-U microscope at 4x magnification at 0, 12, and 24 h after the drug treatment. The percentage of migrated cells was calculated using the equation given below.

$$A_{migrated} = \frac{A_{0-D} - A_{24-D}}{A_{0-C} - A_{24-C}} \times 100\% \text{------- Eq. (3)}$$

$A_{0\text{-}D}$, the area of the scratch in samples treated with drugs at starting time; $A_{24\text{-}D}$, the area of the scratch in samples treated with drugs after 24 h treatment; $A_{0\text{-}C}$, the area of the scratch in samples treated with DMSO at starting time; $A_{24\text{-}C}$, the area of the scratch in samples treated with DMSO after 24 h treatment. The change in the average wound closure is represented by % of wound recovery. Three independent experiments were performed to verify the statistical significance.

2.12. Transwell invasion and migration assay

Article Body Template

The effect of HIC in inhibiting the migration of the PCa cells was done using Transwell invasion assay. The PC3 and DU145 cells at a density of 5×10^5 cells/well was seeded in 500 µl of MEME supplemented with 1% FBS was transferred into the top of chamber of 6-Transwell plates with 8 µm pore size (SPL) with and/or without the presence of HIC and MRS2365. The lower chamber was filled with 2 ml of MEME with 10 % FBS. The plates were kept in the incubator.

For the Matrigel invasion assay, the upper surface of a filter membrane in the upper compartment of a Transwell (pore size, 8 µm) was coated with 200 µl of Matrigel (0.5 mg/ml; Corning, USA) and allowed to settle for 2 h. PCa cells were seeded into the chamber of 6-Transwell plates with the absence and/or presence of the drugs.

After 24 h, the cells that migrate or invade the membranes were fixed in Fixing solution (3.7% paraformaldehyde in PBS) for 15 min. These migrative or invasive cells were dyed with 0.5% crystal violet in 2% EtOH for 30 min. The membranes were then washed thrice with PBS. Five or eight random fields of the membrane were observed under the microscope. Migrated or invaded cells were counted and calculated based on the average of a total number of cells. Data are expressed as the percentage of the number of migrated or invaded cells per field using the below given equation.

$$\%\ of\ invaded\ cells\ = \frac{No.cells_{Drug}}{No.cells_{Control}} \times 100\% \text{ ------- Eq. (4)}$$

No.cells$_{Drug}$ is a number of cells migrated or invaded through the membranes of Transwell under drug treatment. No.cells$_{Control}$ is a number of cells migrated or invaded through the membranes of Transwell upon DMSO treatment.

2.13. Membrane-based antibody microarray analysis

Membrane-based antibody microarrays were done using Proteome Profiler Human phosphorylated kinase Array (cat no. ARY002B) and Proteome Profiler Human NFκB pathway Array (cat no. ARY029) from R&D systems (Boston, USA). The procedure was performed according to the manufacturers' protocol. Briefly, DU 145 cells (5×10^6 cells/ml) were treated with 15.64 µM HIC at 37°C in 5% CO_2 for 48 h. After incubation, the cells were washed twice with cold PBS and the cells were collected by centrifugation. The cells were lysed using lysis buffer supplemented with 2 mM Vanadate, 8.3 µg/mL Aprotinin, 4.2 µg/mL Pepstatin, and 1 mM Trypsin inhibitor (Sigma-Aldrich). Concentrations of soluble cell lysates were measured using AccuOrange™ protein quantitation kit (cat no.30071-T; Biotium, CA, USA). Microarray membranes were blocked with a blocking buffer for 2 h at RT. Then the membranes were simultaneously treated with 200 µg of proteins in cell lysates and a biotinylated antibody cocktail overnight at 4°C. After washing 5 times with washing buffer, the membranes were incubated with streptavidin-conjugated horseradish peroxidase for 2 h at room temperature and washed with washing buffer before detection. The expressions of proteins were detected using ECL

systems (GE Healthcare) with Xenogen IVIS 200 imaging machine (PerkinElmer Inc., MA, USA). The density of protein expressions was analyzed using ImageJ software. The relative level of protein expressions of treated to untreated groups was calculated based on the density of protein expression.

2.14. Statistical analysis

All experiments were performed in triplicates. The results are expressed as mean ± standard deviation (st. dev). Student's t-test and one-way ANOVA analysis was done to prove the significance of the data. The results with $*p < 0.05$ were considered significant confidence intervals. Statistical analyses were performed using Sigma Plot 14 (Systat Software Inc., UK).

3. RESULTS

3.1. The anti-cancer effects of HIC on PCa cells

HIC was found to induce the apoptosis of PC3 and DU145 cell models. To figure out the potential anti-cancer effects of HIC on PCa cell proliferation, the cells were treated for 48 h with the IC_{50} concentration of HIC (Figure 1A) such as 15.98 µM for PC3 and 15.64 µM for DU145 cells, respectively. As shown in Figure 1B, the cytotoxicity effect of HIC reduced the cell density when comparing with DMSO treated cells. Also, PC3 and DU145 cells lost the adherence property and exhibited abnormal morphology upon HIC treatment.

To validate the cytotoxic effect of HIC, clonogenicity assay was performed to identify its ability to reduce the percentage of colonies by inhibiting the proliferation of PCa cells. The PCa cells were treated with the IC_{50} concentration of HIC, MRS2365 as positive control, and DMSO as vehicle control (Figure 1B). The cells resistant to HIC were allowed to grow for 9 days of post treatment. Figure 1C showed the stained colonies having differences in the number and the size of the PCa cells. HIC significantly inhibited the formation of the colonies with about 49.47 ± 2.3% for PC3 and 45.9 ± 7.4% for DU145 than the vehicle control (DMSO) and the positive control (MRS2365). MRS2365 showed comparatively less sensitivity and percentage of inhibition than HIC with about 54.6 ± 11.3% and 52.8 ± 9.9% in PC3 and DU145 cells, respectively (Figure 1D).

3.2. Dose- and Time-Dependent cytotoxicity analysis of HIC in PCa spheroids:

Tumor spheroid model generated from PC3 and DU145 was used as an intermediate in-vitro and in-vivo system to study the anticancer activity of HIC. Dose responsive treatment of HIC on the sphere formation by PCa cells was evaluated by measuring the size of the spheres after 96 h of treatment. The size of the spheres was observed to be indirectly proportional to the increased concentration of HIC. The area of the spheroids was measured using ImageJ software analysis in comparison with the control group. About over 50% of the sphere area was reduced upon 20 µM HIC treatment in both PC3 (Figure 2A) and DU145 cells (Figure 2B). PC3 spheroid area decreased to about 52.4 ± 3.3%, 40.9 ± 3.66% and 20.76 ± 4.8%, whereas DU145 spheroid area showed 84.6

±3.15%, 48.8 ± 2.3%, and 38.23 ± 2.6% upon 5 µM, 10 µM, and 20 µM of HIC treatment, respectively (Figure 2C). Thus, HIC significantly reduced the colonosphere formation in both the PCa cells with the higher effect in PC3 spheroids than the DU145 spheroids.

Meanwhile, time-dependent effect of HIC in the PCa spheroids was analyzed at on day 1, day 3, and day 8 after treatment. MRS2365 was used as a positive control and DMSO as the vehicle control. The spheroid area was reduced in both PCa cells after day 3 of HIC and MRS2365 treatment (Figure 2D and 2E). The size of spheroid was reduced to 52.3 ± 3.1% and 64.3 ± 2.3% for PC3 cells (Figure 2F) and 29.1 ± 2.9% and 57.8 ± 1.6% for DU145 cells on the third and eighth day of treatment, respectively (Figure 2G). MRS2365 also significantly reduced the spheroid area to about 50% after 8 days treatment in both PC3 and DU145 cells. In our previous study, we found that HIC inhibited cell proliferation and induced apoptosis through caspase 3/7 activity and increased ROS production in PCa cells [9]. Similar results were reported by Wei et al., that MRS2365 increases apoptotic cells, caspase 3 activity, and lactate dehydrogenase (LDH) in PC3 cells and thereby inhibits the proliferation of PC-3 cell. MRS2365 was also able to induce ERK1/2 phosphorylation, suggesting its crucial role in prostate cancer signaling pathway [6]. Collectively, our results suggest that HIC could inhibit tumor spheroid models in time- and dose-dependent manner.

3.3. The change of gene expression under HIC treatment

RNA seq analysis was performed to check whether the drug withdrawn PCa cells had any semblance at the transcriptome level with the HIC treated PCa cells. Principal component analysis (PCA) for 19623 genes revealed 3221 DEGs (16.41%) sharing principal components for PC3 and DU145 cell lines suggesting the diverse set of transcriptomic responses upon HIC treatment (Figure 3A and 3B). About 1913 DEGs (9.74 %) were modulated in PC3 cells whereas 1290 DEGs (6.57 %) in DU145, with the significant p-value < 0.05 (Supplementary file 1 and 2). Heat maps were generated for PC3 and DU145 cells illustrating the differential expression data (Figure 3C and 3D). Out of 1919 DEGs in PC3 cells, 576 genes were upregulated, and 391 genes were downregulated with significant fold change between HIC and DMSO treated group (Figure 3E). Likewise, DU145 showed 530 upregulated DEGs and 635 DEGs downregulated genes (Figure 3F).

3.4. Inhibition of HIC on dynamic cellular damage

The differentially expressed transcripts were categorized through PANTHER annotation tool where enrichment analysis of biological processes was performed to determine the potential GO and KEGG pathways regulated by HIC treatment. We could observe a few GO biological processes related to DNA replication, damage response in signal transduction by p53 class mediator, polymerase binding, G1/S phase DNA damage, and DNA repair regulated under HIC treatment in PC3 and DU145 cells (Figure 4A and 4B). For a deeper insight, we also have analyzed the key

genes regulated in DNA damage process upon HIC treatment in both PCa cells. The top up-regulated genes in PC3 treated cells include *CDKNIA*, *CCNB3*, *NBR2*, *UVSSA* while top down-regulated genes were *SOX4*, *MDM2*, MDM4, *TP73*, *CDK1*, *TUBA1A* and *TUBA1B* involved in DNA damage (Figure 4C). Similarly, DU145 cells, HIC revealed up-regulation of *TEP1*, *UVSSA*, and *NBR2* genes while down-regulated genes include *TUBA 1A*, *TUBA 1B*, *TP73*, *SOX4*, *CDK1*, *CDK2*, *MDM2,* and *MDM4* (Figure 4D). *CDK1* [35] and *CDK2* [36] downregulation play a central role in DNA damage-induced cell cycle arrest and DNA repair. Also, downregulation of *SOX4* expression intends to the inhibition of cell apoptosis, increase cell invasion and metastasis, and maintain cancer-initiating cells. In addition, *TP73* and *SOX4* were reported their function related to the p53 signaling pathway. Based on the activation of p53, HIC can induce cell stress signals such as cell death, DNA damage, oxidative stress [37,38].

Downregulation of *MDM4* and *MDM2* regulates p53 activity and stability, thus enhances DNA damage and reduces cell survival. [39,40]. Furthermore, the upregulation of *CDKN1A* was observed coding for p21 protein, which is responsible for the DNA damage and further activates G1-phase cyclin/CDKs complexes [41]. Thus, HIC found to regulate the genes involved in DNA damage through the activation of p52-p21 signaling in both the PCa cell lines.

Furthermore, we also analyzed KEGG analysis reflecting the functional pathways and GO annotation representing the molecular functions upon HIC treatment in both the cell lines. Depending on the lists of GO biological processes, MAPK and NF-κB signaling pathways were noted as the potential regulations in HIC conditions when compared to the vehicle groups

(Supplementary files 3 and 4). Moreover, KEGG pathway regulated by HIC treatment in both cell lines were listed in Figure 4E and 4F. HIC was deemed to be highly related to p53 signaling pathway, cell cycle arrest, and DNA damage. Taken together, these results suggest the hypothesis that p53 mediates the DNA damage, whereas MAPK and NF-κB signaling pathway might be potentially regulated by HIC in PCa cells.

3.5. The activity of HIC through apoptotic response and G1/S cell cycle arrest in PCa cells

Several reports have shown that the activation of $P2Y_1R$ induces cell death in PCa cells [6,8,9]. The process of apoptosis is a double-edged sword, thus targeting the defect or abnormality in the apoptotic pathway might be an interesting factor for cancer treatment. Thus, Annexin V-FITC apoptosis assay was performed to investigate the anti-cancer effect of HIC on PCa cells. Cells that are fluorescent bright red represent necrotic cells whereas cells in fluorescent bright green are positive to apoptotic process. As shown in Figure 5A, PC3 and DU145 cells treated with HIC, showed a greater number of cells entering apoptosis than vehicle groups. In order to pursue more insights on the apoptosis effect of HIC, we also performed microarray analysis where key DEGs involved in apoptotic process were listed in Figure 5B. Upon HIC treatment, key DEGs involved in apoptotic process such as *BAX* and *CDKN1A* were upregulated in both the PCa cells. *BAX* is known as the mediator of tumor suppressive p53 in cancer [42]. Also, downregulation of several survival genes such as *MYD88*, *MDM2*, *MDM4,* and *TLR3* was also noticed in both the

cells. MYD88 protein functions as a negative regulator of TLR3 which is essential in restricting TLR3 signaling and thereby protects the host from unwanted immunopathologies associated with the excessive production of IFN-β [43]. MDM2 and MDM4 proteins negatively correlate with the expression of CDK inhibitor, and directly interact with p21 and p53 protein and hence promote the degradation. These observations suggest that the apoptotic phenomena induced by HIC in PCa cells might relate to not only p53 signaling but also p21 pathways in both PC3 and DU145 cells. DNA damage and apoptosis response have been known to regulate the cell cycle arrest and cell proliferation [44]. In this study, cell cycle analysis was done to identify the effect of HIC arresting the cells at different phases of cell division. As shown in Figure 5C and 5D, microscopic images revealed the fluorescence bright red colored cells which are proportionate to the DNA content in different phases of cell cycle. The percentage of PC3 cells in G1 phase significantly increased to 52.3% and 65.9% when treated with HIC and MRS2365 respectively, with 34.5% for vehicle control (Figure 5E). The transition of PC3 cells to S phase was not significant among the samples which showed 16.9%, 15.4%, and 8.2% upon DMSO, HIC, and MRS2365 treatment, respectively. Likewise, the percentage of DU145 cells in G1 phase was about 46.7%, 38.5%, and 32.4% upon HIC, MRS2365, DMSO treatment respectively. Also, 46.7%, 38.5%, and 32.4% of DU145 cells in S phase was observed when treated with HIC, MRS2365, DMSO respectively (Figure 5E). It was observed that a higher fraction of cells was arrested at the proliferative G1 phase in PC3 cells and at G1/S phase in DU145 cells upon HIC treatment.

There are several biological processes involved in cell cycle pathway that were either inhibited or enhanced by HIC treatment in PC3 and DU145 cells (Supplementary files 3 and 4). Based on the above-mentioned data, the genes involved in G1/S phase were selectively analyzed which were represented in Figure 5F. In both PC3 and DU145 cells, *MCMs, CDKN1A,* and *CDK2* expression were reduced by HIC. Down-regulation of *MCMs* (*MCM2* and *MCM4* in PC3 cells and *MCM3*, *MCM4*, and *MCM6* in DU145 cells) were known as the crucial components which restrict the DNA elongation and thus inhibits the proliferation at G1 phase [45]. In addition, HIC reduced the expression of *CCNE2* and *CCNA2* in DU145 cells. Cyclin E (*CCNE2*) and Cyclin A (*CCNA2*) are known as essential stimulators for G1/S phase initiation and activate Cdk2 for initiation of DNA replication [46]. The downregulation of *CDK2* triggers the G1/S checkpoint through the activation the p53-p21 pathways [47]. Also, HIC increased the expression of *CDKN2A* and *CDKN2B* which were the tumor expression genes in G1/S phase arrest [48]. Based on the gene expression data, the p53 activation and downregulation of Cyclins and cyclin-dependent kinase were determined under HIC treatment in both cell lines. Collectively, the results suggest that HIC suppresses the G1 progression in PC3 cells and G1/S transition in DU145 cells. The induction of G1/S phase arrest may be associated with the inhibitory effects of HIC on cancer cell growth and the activation of $P2Y_1R$ on cell apoptosis.

3.6. The anti-metastasis effects of HIC on PCa cells

Article Body Template

Several studies have been reported that $P2Y_1R$ mediates both cell growth and/or decreases cell proliferation in different cell lines [11,13,20]. Here, we performed the cell migration and invasion assay to investigate the effect of HIC on PCa cell metastasis. The ability of HIC in inhibiting the migration of PC3 and DU145 cells was examined by wound-healing assay. The cells were treated with the IC_{50} concentration of HIC on each cell line, where the drug reduced the wound closure ability in a time-dependent manner when compared to the vehicle (Figure 6A and 6B). After 12 h of treatment, a similar pattern of inhibition of migration was observed in both cells upon HIC and MRS2365 treatment. However, after 24 h HIC inhibited more cell migration than MRS2365 in both PC3 and DU145 cells. The wound area recovery was calculated for both PC3 and DU145 cells to compare the efficiency of HIC and MRS2365 as an anti-metastasis agent. PC3 cell showed about 20.19 ± 9.03% and 21.05 ± 9.2% of recovery area at 12 h, whereas 37.15 ± 7.32% and 50.31 ± 7.18% at 24 h for HIC and MRS2365, respectively (Figure 6C). Similarly, in DU145 cells, the wound recovery rate of HIC and MRS2365-treated cells after 12 h was 20.08 ± 11.75% and 24.76 ± 12.21%, respectively. After 24 h, HIC showed 39.78 ± 7.68% migrated area whereas MRS2365 presented the higher migrated area of about 64.23 ± 6.77% (Figure 6D).

Consistently, Transwell migration assay confirmed the above observations in which migrated cells were effectively reduced in the presence of HIC. The PCa cells were plated in 1% FBS medium in the upper chambers with and/or without drugs for 24 h. The Transwells along with migrated cells were stained with crystal violet and shown in Figure 6E. Compared to the vehicle group, about 45.1 ± 5.52% and 55.7 ± 5.95% reduction in the migration of PC3 and DU145 cells was

observed when treated with HIC, respectively (Figure 6F). Thus, the results indicated that HIC effectively reduced the movement of PC3 and DU145 cells. To further determine the inhibitory effect of HIC on the invaded cells, PCa cells were treated with the drug and the cells were allowed to invade in Matrigel-coated Transwell for 24 h (Figure 6G). HIC suppressed the invasion by 55.1 ± 5.96 % and 50.8 ± 8.81% in PC3 and DU145 cells respectively when compared to the untreated group (Figure 6H). These data clearly showed that HIC could strongly suppress the PCa cell invasion.

To explore the effect of HIC in detail, gene expression analysis was carried out simultaneously. Genes associated with the cell migration and invasion were listed in the Figure 6I and 6J. Here, the top 20 DEGs in PC3 and DU145 cells were reported upon HIC treatment. In both PCa cells, the expression of *TGFB2*, *TGFB3*, *MEF2C*, *ANXA3*, *SCG2, HMGB1* and *BMP4* was downregulated by HIC treatment. Among these genes, *TGFB2* and *TGFB3* belong to transforming growth factor β (TGF-β)-a multifunctional cytokines family that promotes invasiveness and angiogenesis in tumor cells [49]. *MEF2C* transcription factor was known to induce epithelial mesenchymal transition (MET) and invasiveness of carcinoma through the activity of TGF-β [50]. In addition, the downregulation of ANXA3 and BMP4 proteins suppresses tumor metastasis and decreased the proliferation of cancer cells through the inhibition of matrix metalloproteinases (MMPs) [51,52]. Indeed, SCG2, secretogranin II gene encoding for the motility-related protein SgII, is highly expressed in cancer tissue and involved in cancer cell migration[53]. Also, High mobility group box 1, HMGB1, is also upregulated in several type of cancers whereas its downregulation inhibits

cell proliferation, migration and invasion [54]. Thus, the downregulation SCG2 and HMGB1 protein in PC3 cells was observed upon HIC treatment suggesting the crucial role of HIC on prostate cancer cell migration. Similarly, HIC downregulated the expression Sox4, MDM2, MDM4 in both the cell lines, PC3 and Du145 which could inhibit cell proliferation, migration and apoptosis induction thus regulating p53 activity. Notably, in human cancers downregulation of wild-type p53 function is inhibited by high levels of MDM2 and MDM4, which in turn lead to the downregulation of tumor suppressive p53 pathways. Thus, the inhibition of MDM2 and MDM4-p53 interaction regulates p53 activity and stability, thus enhances DNA damage and reduces cell survival and hence presents an appealing therapeutic strategy for the treatment of cancer [55]. Collectively, the results suggest that HIC negatively affects cell metastasis through the regulation with TGF-β and p53 pathways in PCa cells.

3.7. Regulation of HIC on MAPK and NF-κB signaling pathway

The association of $P2Y_1R$ in the activation of NF-κB - MAPK signaling prompted us to examine the effect of HIC on the respective protein expression profiling. We selected DU145 cells for these mechanistic studies as HIC seemed to be more effective in suppressing the growth and inducing G1/S phase arrest of cell cycle progression. To identify which phosphorylated kinase significantly stimulated by HIC, protein profiling of human phospho-MAPK protein array using DU145 cell line was done. DU145 cells were treated with HIC with DMSO as vehicle control, then the samples were tested for the differential expression of phosphorylated kinases. Twenty-four differentially phosphorylated kinases were spotted in the phosphor-MAPK array. The change in the expression

of very few kinases was observed between HIC- and DMSO-groups (Figure 7A) and the fold change of phosphorylation level with *p-value < 0.05 was presented in Figure 7B. Increased expression of ERK1/2, JNK1/2, and AKT phosphorylation was observed in HIC treated cells. The fold changes in the signal intensity of phosphorylated proteins like ERK1, ERK2, JNK1, JNK2, and AKT (Ser473) were found to be 1.1, 1.21, 1.11, 1.09, and 1.08, respectively. These results were consistent with the function of $P2Y_1R$ that up-regulated the activated form of ERK1/2, JNK1/2, and AKT. Conversely, phosphorylation of p38 and MKK3/6 remained unchanged over basal levels by HIC treatment in comparison with DMSO group. ERK1/2 activation was known to regulate to p53 signaling-dependent G1 arrest, which mediates either cell growth or apoptotic response based on the downstream targets [56–58]. In addition, JNK1/2 was demonstrated to stimulate p53 signaling and the downstream target of p53 [59–61]. p53 pathway was reported as the essential tumor suppression for cell apoptosis, G1 arrest cell cycle, and cell proliferation [62]. To get more insight into the modulation of $P2Y_1R$ on NF-κB pathway, we performed a proteome profiler array to identify the differential expression of proteins of NF-κB signaling upon HIC treatment. Almost 5 out of 27 proteins were expressed differentially in HIC- and DMSO-treated groups (Figure 7C) with $p < 0.05$. Protein p53 and phosphorylated protein p53-Ser46 were increased with the fold change of 1.11 and 1.24 respectively for HIC- and DMSO-groups (Figure 7D). One of the most important p53 functions is its ability to activate apoptosis through transcription-dependent and -independent mechanisms. Moreover, the phosphorylated form of p53 at Ser46 enhances apoptosis by activating pro-apoptotic target gene transcription. The levels

of IL-1, STAT1, and STAT2 proteins were slightly increased by HIC with the fold change 1.02, 1.05, and 1.03, respectively. Interestingly, the protein expression of I-κB, NF-κB remains unchangeable on HIC treatment. Collectively, the results suggest that HIC could suppress the proliferation of cancer cells through ERK1/2, JNK, and p53 signaling pathways.

4. DISCUSSION

Several studies have shown that $P2Y_1R$ has the dual function in promoting or inhibiting cancer cell proliferation and metastatic [20,22,63]. Our previous report has shown that HIC, a selective agonist of $P2Y_1R$, reduces the PCa cell growth in a time- and dose-dependent manner [9]. In addition, HIC promotes cell apoptosis by increasing the activity of caspase 3/7 and ROS productivity.

In this study, we performed several experiments to investigate the mechanism and anti-cancer effects of HIC in PC3 and DU145 cell models. HIC was found to inhibit colony formation and cell proliferation in PCa cells (Figure 1). Moreover, the results indicated that HIC exhibited antitumor activity by reducing spheroid areas in a time- and dose-dependent manner in a system that more closely resembles the in *vivo* setting (Figure 2). GO analysis revealed the list of up- and down-regulated genes by HIC in DNA replication, DNA damage in response to signal transduction by p53 tumor suppressor and p21, G1/S arrest phase DNA damage (Figure 3 and 4). Thus, DNA damage was induced in both PC3 cells and DU145 cells by HIC treatment related to p53 signaling. Our data also showed the anti-cancer activity of HIC through the apoptosis, G1/S phase arrest,

and p53 upregulation in both PCa cells (Figure 5). Apoptotic response was then determined with the down-regulated genes such as *MYD88*, *FOS*, *MDM2*, *MDM4,* and *TLR3* and up-regulated genes such as *BAX*, *CDK1A*, and *FBXO*. MDM2 and MDM4 proteins were known to increase p53 protein degradation whereas BAX is the crucial mediator for proapoptotic signaling through the activation of p53 [39,64,65]. In addition, HIC induces cell cycle arrest at G1 phase of PC3 cells and G1/S phase of DU145 cells, through the downregulation of *Cdks*. We found that HIC-induced both PCa cell cycle arrest at G1 phase, which was associated with downregulation of *CDK1*, *TP73*, *MCM4*, *MCM6* levels. In addition, *Cyclin E* and *Cyclin A*, essential stimulators for G1/S progression of cell cycle, were decreased by HIC in DU145 cells [66]. Besides, the anti-metastasis effects of HIC on PCa cells was observed through the inhibition of migrated and invaded cells. The genes involved in metastasis process were found to be downregulated for *TGB2*, *TGFB3*, *MEF2C*, *ANXA3*, and *BMP4* under HIC treatment. These genes regulate to TGF-β receptor and increase the metastasis process in cells [49–52]. Several studies have been reported that the cross-talk between p53 and TGF-β signaling regulates cell growth and cell phase arrest [67,68]. Collectively, HIC might induce p53 signaling and promote the cell death through its activation.

Multiple signaling pathways have an influence on p53 activation, such as MAPKs and NF-κB pathways [69]. $P2Y_1R$ activation also induces the phosphorylation of ERK1/2 and JNK1/2 and involves NF-κB pathways in cancer and inflammation [70,71]. MAPK signaling has been known to promote either cell growth or cell apoptosis based on the cell types and catalysts [18]. Especially, ERK1/2 activation is linked with the subsequent phosphorylation and stabilization of p53 for

apoptosis [22,56–58]. In addition, JNK1/2 has been reported to directly or indirectly modulate p53 and its down-stream targets in cell death [19,59–61]. Here, we found that the protein levels of ERK1/2 and JNK1/2 phosphorylation were increased by HIC in DU145 cells. These results were consistent with the hypothesis that $P2Y_1R$ could regulate p53 stabilization through the activation of ERK1/2 and JNK1/2 [19]. The stabilization of p53 protein inducing DNA damage, G1/S phase arrest could decrease the expression of cancer genes that is conducive to cancer metastasis [72]. In addition, the protein expression of I-κB and NF-κB remains unchangeable whereas IL-1 expression was slightly increased with the fold change of about 1.03 in NF-κB protein array. Therefore, the regulation between NF-κB signaling through the activation of $P2Y_1R$ by HIC was not observed in PCa cells. However, the fold change of p53 and p53-Ser46 proteins was increased by HIC condition. These proteins promote apoptosis through the activation of pro-apoptotic target transcription [72]. In addition, our previous study presented that $P2Y_1R$ activation increased the Ca^{2+}, caspase 3/7 activity, and ROS levels in PC3 and DU145 cells. Ca^{2+}, PKC-α, and PKC-δ are important $P2Y_1R$ secondary messengers that help in MAPK activation [73–75]. Ca^{2+} levels directly increase the phosphorylation level of ERK1/2 in mammalian cell models [76]. Moreover, PKC-α is known as a mediator for p53 activity, which plays a crucial role in preventing cell growth by ADP and 2-MeSADP, agonists of $P2Y_1R$ [19,73].

Overall, our results suggest the new sights of HIC in PCa treatment. HIC induces apoptosis and cell cycle arrest by modulating $P2Y_1R$ activation and p53 signaling pathway. The anticancer effect

of HIC on inhibiting PCa cells growth and spheroid development implies HIC as a potential cancer therapeutic. Therefore, HIC can be developed as an anticancer agent against PCa proliferation.

5. CONCLUSION

Overall, our findings are consistent with the earlier studies on the anti-cancer effect of P2Y1 agonists in cancer cells and in PCa cells. HIC regulates the several genes involved in DNA damage, the major checkpoints in cell cycle, apoptotic response, and metastasis. Additionally, HIC inhibits cell proliferation and migration through the modulation of MAPKs and p53 signaling pathways. Thus, HIC can be developed for the treatment of PCa.

6. FUTURE PERSPECTIVE

Prostate cancer is the second most leading cause of cancer-related death in men. Surgery in combination with radiation therapy, chemotherapy and hormonal therapy is the main mode of treatment for PCa. New treatment regimens are pursued to extend the survival of cancer patients with metastasis. The present research on the P2Y1R and HIC mediated cell death and apoptosis will provide the therapeutic advances on PCa treatment. The regulation of P2Y1R activation and stabilisation of p53 protein by HIC might improve the understanding of cell proliferation and DNA damage in PCa treatment. The evidence provided by the present research on cellular migration and invasion, gene expression analysis and cell cycle analysis might increase the therapeutic implications for advanced prostate cancer treatment.

Article Body Template

Executive Summary Points

1. The functional activity of 1-(2-hydroxy-5-nitrophenyl)(4-hydroxyphenyl)methyl)indoline-4-carbonitrile (HIC), an agonist of P2Y1 receptor (P2Y1R) was evaluated.
2. HIC reduced the cell proliferation, adherence property and spheroid formation of PC cells
3. HIC was able to arrest the cell cycle at G1/S phase and induces apoptosis.
4. HIC regulates the downstream signaling pathways of prostate cancer cells
5. HIC affects p53, mitogen-activated protein kinase (MAPK), and nuclear factor kappa-light-chain B (NF-κB).
6. HIC activated the phosphorylation of ERK1/2 and JNK1/2, p53, and p53-ser46 proteins
7. HIC agonist function as a p53 stabilizer for prostate cancer cell death induction

Article Body Template

Figures:

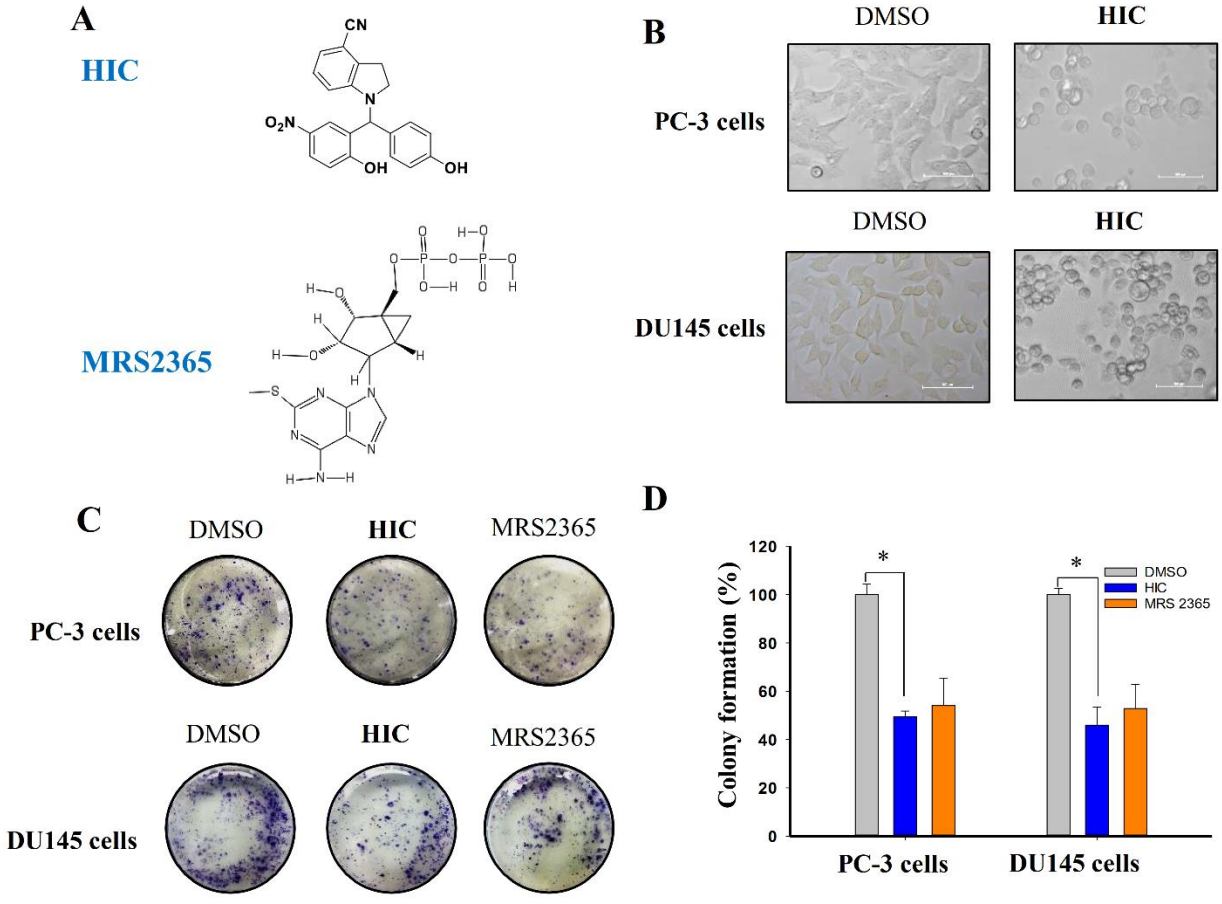

Figure 1: The anti-cancer effects of HIC on PCa cells through P2Y$_1$R activation. (A) Chemical structure of HIC and MRS2365. (B) Clonogenicity assay on PCa cells treated with the IC_{50} concentration of HIC, where MRS2365 used as the positive control, and DMSO as the vehicle control. (C) The colony-forming ability of the PCa cells at 48 h stained with crystal violet were imaged under fluorescent microscope at 20x magnification (scale bar = 100 µm). (D) The bar

graph showed the percentage of colony formation in PCa cells treated with HIC and/or MRS2365 treatment after 9 days, with DMSO control (vehicle control) ($n = 6$, $*p < 0.05$).

Article Body Template

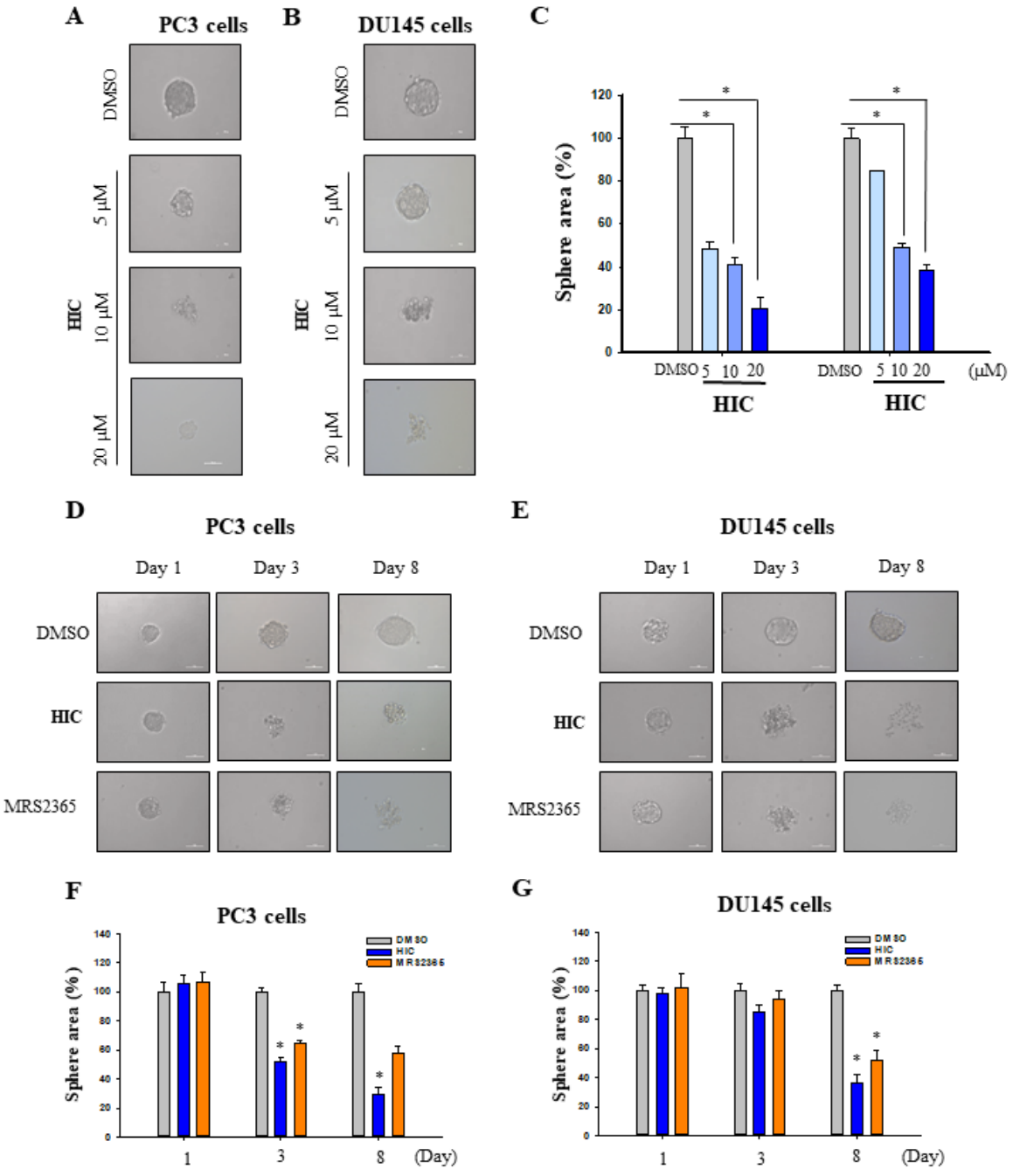

Figure 2: The inhibitory effects of HIC on spheroid growth in a dose- and time-dependent manner. Effect of HIC on spheroid formation in (A) PC3 and (B) DU145 cells upon varying concentrations, with DMSO as the vehicle control (C) Spheroid area (μm^2) upon concentration dependent HIC treatment in both PCa cells, where there is significant difference when compared with DMSO. (E) Time-dependent effect of HIC in the PCa spheroids was analyzed at day 1, 3 and 8 with DMSO as a vehicle control and MRS2365 as the positive control. Spheroid area (μm^2) upon time dependent HIC treatment in (F) PC3 and (G) DU145 cells. All experiments were performed with three independent times. Significant data were denoted by $*p < 0.05$ using student's t-test.

Article Body Template

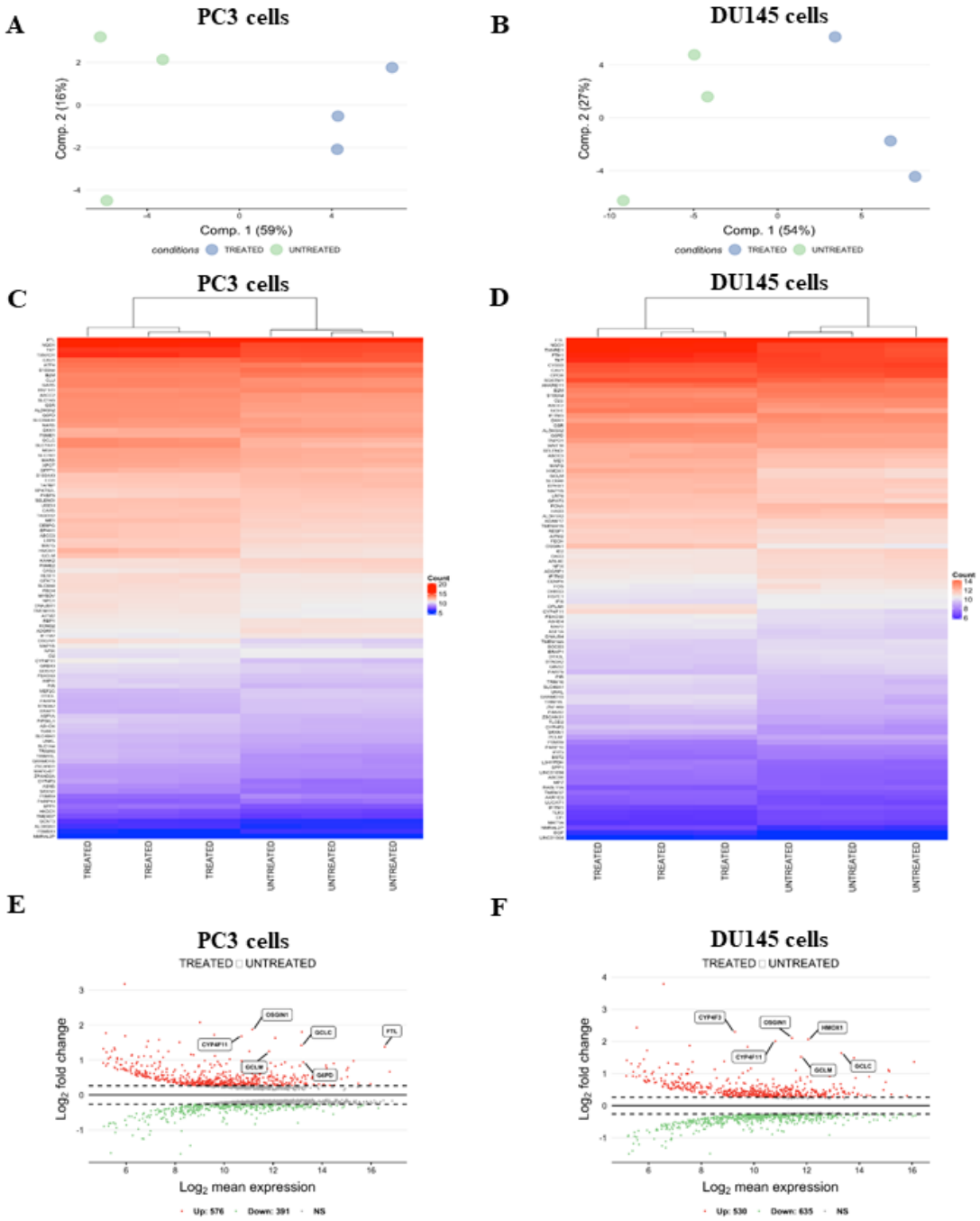

Figure 3: Analysis of gene expression in PCa cells upon HIC treatment. Gene expression modulation between HIC-treated group and DMSO-vehicle group in (A) PC3 cells and (B) DU145 cells. Heat map generated by R program represents the difference in the expression levels of genes (C) for PC3 cells and (D) for DU145 cells. Higher and lower levels of transcript accumulation are indicated by blue and red color, respectively, whereas white stripes indicate the median level of expression. The fold change of genes was represented in red color dots for up-regulated expression and green dot for down-regulated expression (E) in PC3 cells and (F) DU145 cells. The data were normalized and considered significant with $*p < 0.05$.

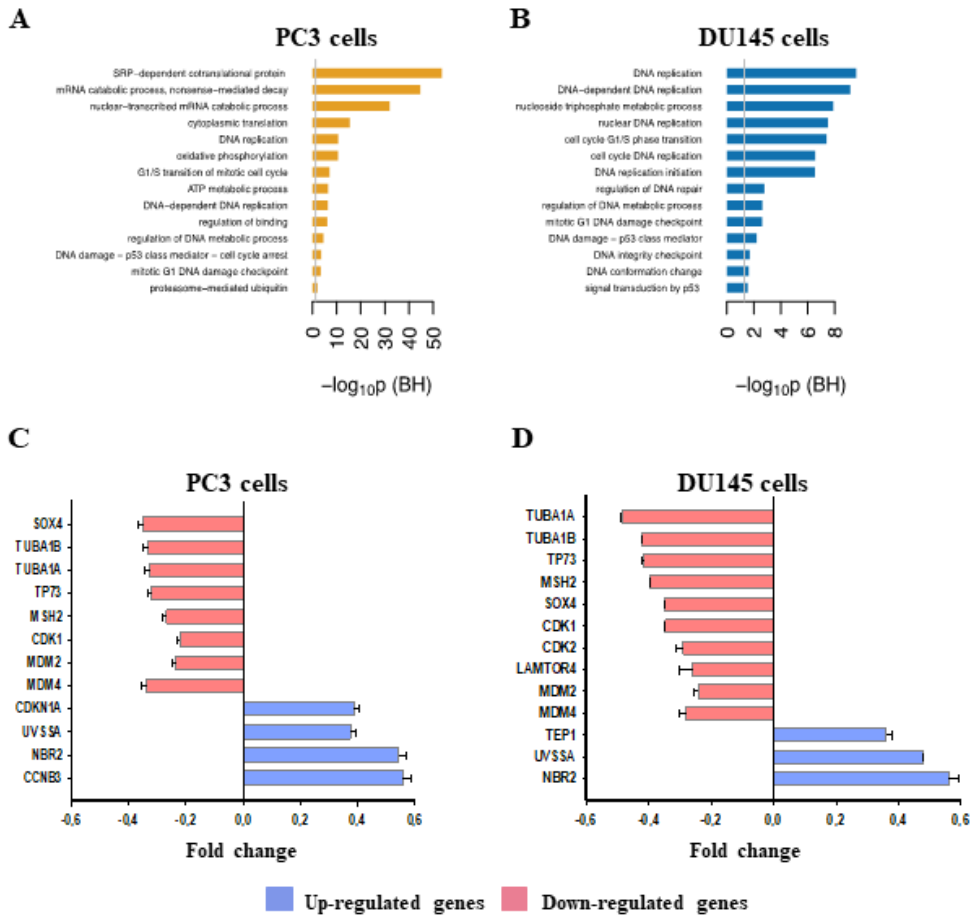

E

KEEG Pathway	Value	p-value
DNA replication	1,78E-11	4,74326E-09
Oxidative phosphorylation	1,53908E-08	1,90762E-06
Cell cycle	1,58478E-07	1,05513E-05
p53 signaling pathway	0,003080914	0,038714185
Mismatch repair	0,001291764	0,02293448

F

KEEG Pathway	Value	p-value
Oxidative phosphorylation	8,98472E-11	8,25964E-09
Protein processing in endoplasmic reticulum	5,66993E-09	3,90927E-07
DNA replication	1,71169E-07	5,24518E-06
Cell cycle	0,00058759	0,011575074
Ribosome	9,63442E-35	2,65707E-32

Figure 4: Inhibition of HIC on dynamic cellular damage. Genome annotation using PANTHER was done in (A) PC3 cells and (B) DU145 cells. The top DEGs involved in the DNA damage upon HIC treatment (C) in PC3 cells and (D) in DU145 cells were represented as color coded graph with red

for red for down-regulated genes and blue for up-regulated genes. KEGG pathway regulated by HIC treatment in were listed in (E) in PC3 cells and (F) in DU145 cells. The expression of DEGs were considered significant with $*p < 0.05$.

Article Body Template

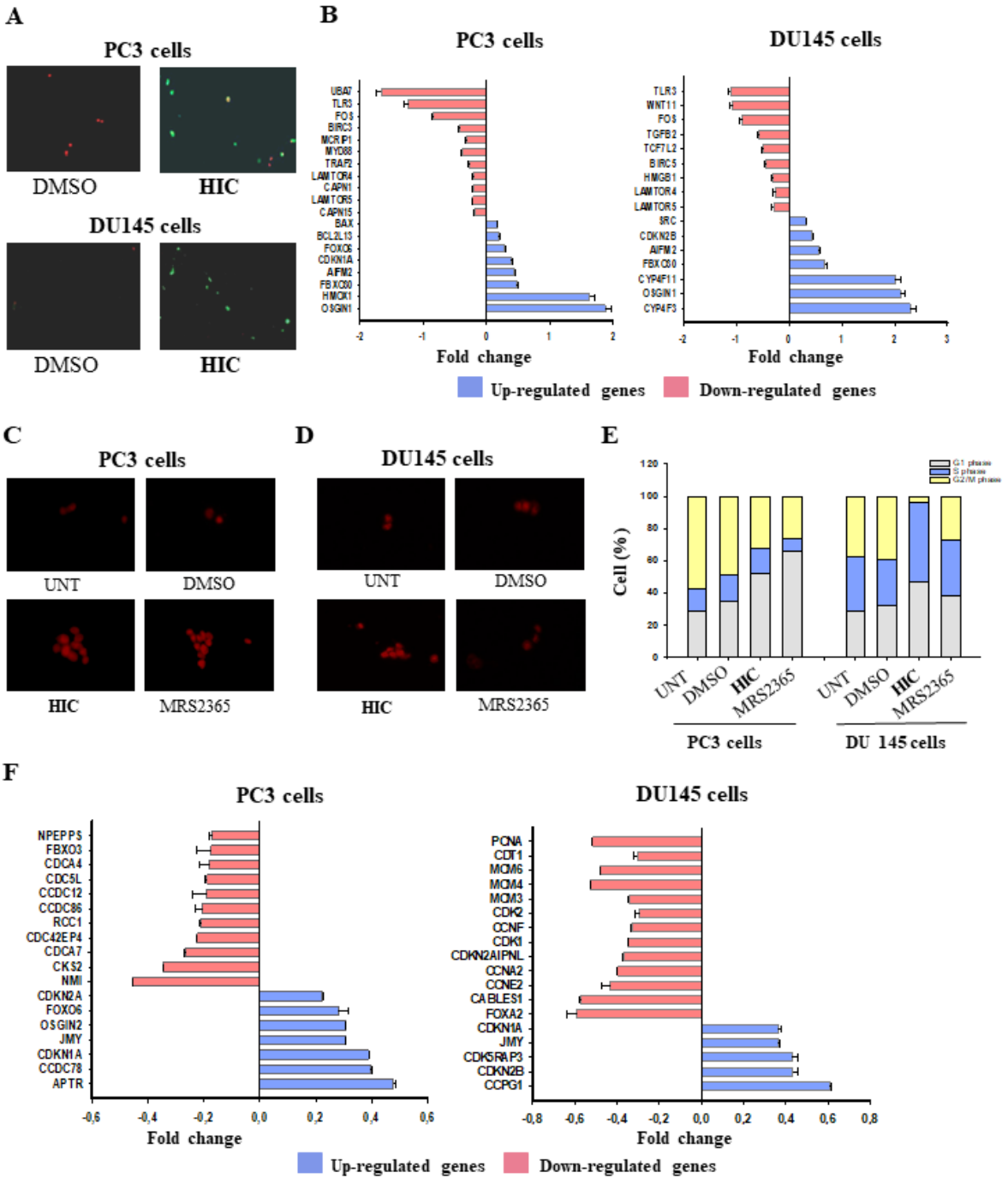

Figure 5: The activity of HIC through apoptotic response and G1/S cell cycle arrest in PCa cells. (A) Microscopic images of PC3 and DU145 cells stained with Annexin-V/PI upon HIC treatment with DMSO as vehicle control. (B) Top DEGs associated with apoptosis regulated by HIC treatment for PC3 and DU145 cells were represented as color coded graph. Propidium iodide staining of (C) PC3 and (D) DU145 cells upon HIC treatment with MRS2365 and DMSO as control. (E) Percentage of dividing cells in each phase of the cell cycle determined by MATLAB R2013b (*t*-tests, n = 6). (F) Key genes involved in cell cycles arrest and their fold-changes with color coded graph.

Article Body Template

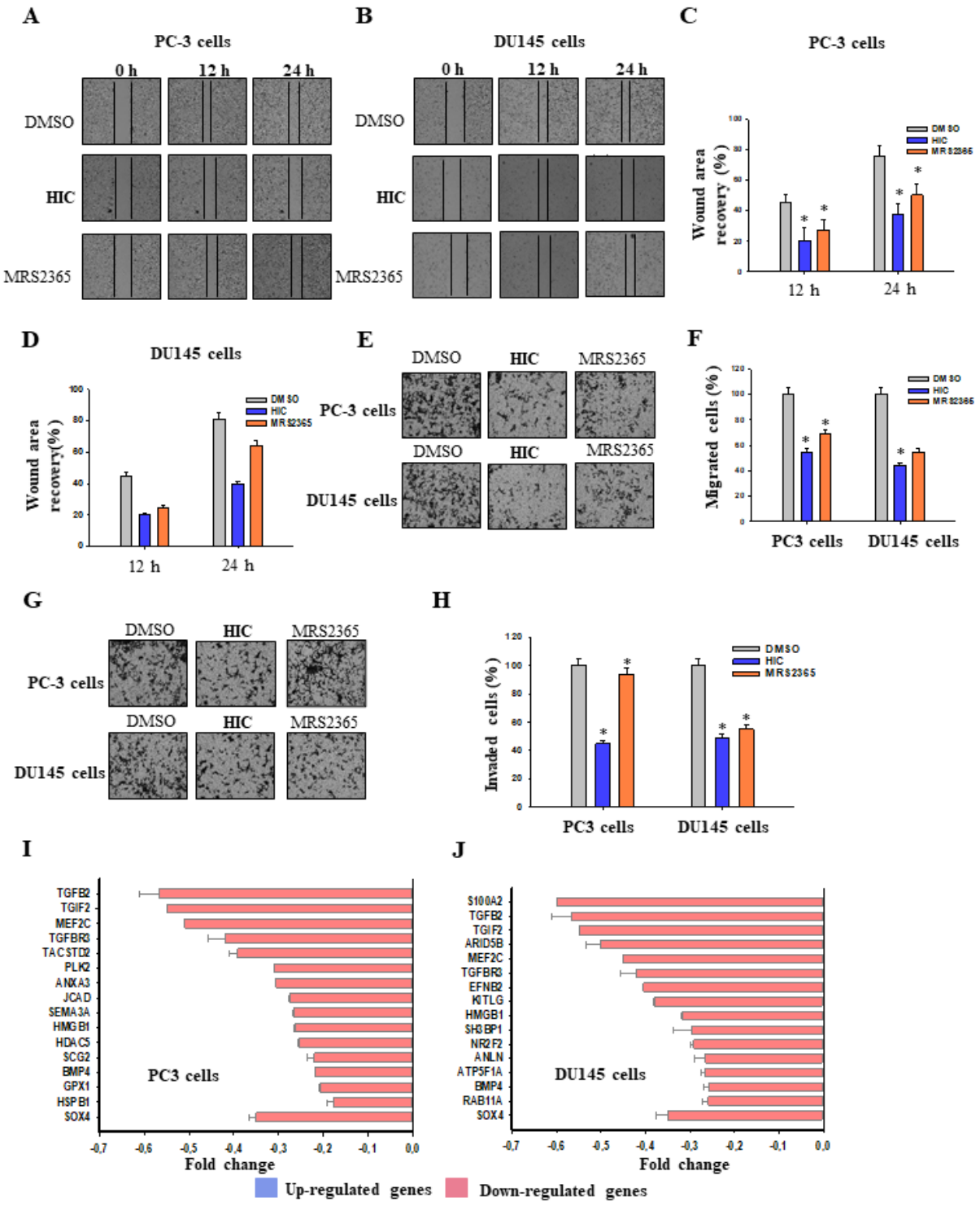

Figure 6: The anti-metastasis effects of HIC on PCa cells. Wound healing assay showing the ability of HIC in inhibiting the migration of (A) PC3 and (B) DU145 cells at different time points like 0 h, 12 h and 24 h. Percentage of wound area recovery was calculated for (C) PC3 and (D) DU145 cells upon HIC with MRS2365 as positive control and DMSO as vehicle control. (E) Microscopic images of HIC treated PCa cells showing Transwell migration assay. (F) Percentage of inhibition of migration of PCa cells after HIC treatment. (G) Microscopic images of PCa cells in Matrigel-coated Transwell representing the invaded cells. (H) Percentage of inhibition of invasion of PCa cells after HIC treatment. Top DEGs associated with the cell migration and invasion in (I) PC3 and (J) DU145 upon HIC treatment was represented in color coded graphs.

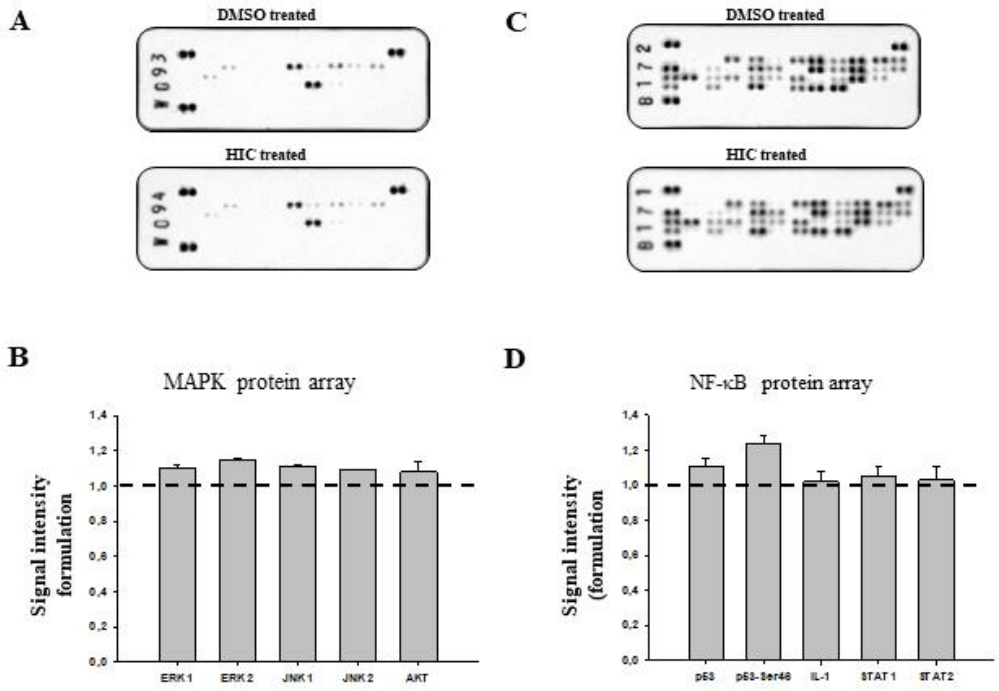

Figure 7: Regulation of HIC on MAPK and NF-κB signaling pathway. (A) phospho-MAPK protein array analysis in DU145 cells treated with HIC after 48 h. (B) The bar chart show the relative density of expression of proteins of MAPK between HIC treated groups and DMSO groups. (C) NF-kB protein array analysis in DU145 cells treated with HIC after 48 h. Images were captured using Xenogen IVIS 200 imaging system. (D) Bar diagram shows the relative expression of NF-kB protein with the percentage changes in luminescence intensity relative to DMSO control.

REFERENCES

1. Attard G, Parker C, Eeles RA, *et al.* Prostate cancer. Lancet (2016).

2. Litwin MS, Tan HJ. The diagnosis and treatment of prostate cancer: A review. JAMA - J. Am. Med. Assoc. (2017).

3. Yu S, Sun L, Jiao Y, Lee LTO. The role of G protein-coupled receptor kinases in cancer. Int. J. Biol. Sci. (2018).

4. Saengsawang W, Rasenick MM. G Protein-Coupled Receptors. In: *Encyclopedia of Cell Biology* (2016).

5. Janssens R, Communi D, Pirotton S, Samson M, Parmentier M, Boeynaems JM. Cloning and tissue distribution of the human P2Y1 receptor. *Biochem. Biophys. Res. Commun.* (1996).

6. Wei Q, Costanzi S, Liu QZ, Gao ZG, Jacobson KA. Activation of the P2Y1 receptor induces apoptosis and inhibits proliferation of prostate cancer cells. *Biochem. Pharmacol.* (2011).

7. Li WH, Qiu Y, Zhang HQ, *et al.* P2Y2 receptor promotes cell invasion and metastasis in prostate cancer cells. *Br. J. Cancer*. (2013).

8. Shabbir M, Ryten M, Thompson C, Mikhailidis D, Burnstock G. Characterization of calcium-independent purinergic receptor-mediated apoptosis in hormone-refractory prostate cancer. *BJU Int.* (2008).

9. Le HTT, Rimpilainen T, Konda Mani S, *et al.* Synthesis and preclinical validation of novel P2Y1 receptor ligands as a potent anti-prostate cancer agent. *Sci. Rep.* (2019).

10. Buvinic S, Bravo-Zehnder M, Boyer JL, Huidobro-Toro JP, González A. Nucleotide P2Y1 receptor regulates EGF receptor mitogenic signaling and expression in epithelial cells. *J. Cell Sci.* (2007).

11. Woehrle T, Ledderose C, Rink J, Slubowski C, Junger WG. Autocrine stimulation of P2Y1 receptors is part of the purinergic signaling mechanism that regulates T cell activation. *Purinergic Signal.* (2019).

12. Niimi K, Ueda M, Fukumoto M, *et al.* Transcription factor FOXO1 promotes cell migration toward exogenous ATP via controlling P2Y1 receptor expression in lymphatic endothelial cells. *Biochem. Biophys. Res. Commun.* (2017).

13. Mamedova LK, Gao ZG, Jacobson KA. Regulation of death and survival in astrocytes by ADP activating P2Y1 and P2Y12 receptors. *Biochem. Pharmacol.* (2006).

14. Harden TK, Waldo GL, Hicks SN, Sondek J. Mechanism of activation and inactivation of Gq/phospholipase C-B signaling nodes. Chem. Rev. (2011).

15. Mizuno N, Itoh H. Functions and regulatory mechanisms of Gq-signaling pathways. NeuroSignals (2009).

16. Xu KP, Dartt DA, Yu FSX. EGF-induced ERK phosphorylation independent of PKC isozymes

in human corneal epithelial cells. *Investig. Ophthalmol. Vis. Sci.* (2002).

17. Yin J, Yu FSX. ERK1/2 mediate wounding- and G-protein-coupled receptor ligands - Induced EGFR activation via regulating ADAM17 and HB-EGF shedding. *Investig. Ophthalmol. Vis. Sci.* (2009).

18. Sun Y, Liu WZ, Liu T, Feng X, Yang N, Zhou HF. Signaling pathway of MAPK/ERK in cell proliferation, differentiation, migration, senescence and apoptosis. J. Recept. Signal Transduct. (2015).

19. Muscella A, Cossa LG, Vetrugno C, Antonaci G, Marsigliante S. Inhibition of ZL55 cell proliferation by ADP via PKC-dependent signalling pathway. *J. Cell. Physiol.* (2018).

20. Wong PC, Watson C, Crain EJ. The P2Y1 receptor antagonist MRS2500 prevents carotid artery thrombosis in cynomolgus monkeys. *J. Thromb. Thrombolysis*. (2016).

21. Li Y, Yin C, Liu P, Li D, Lin J. Identification of a Different Agonist-Binding Site and Activation Mechanism of the Human P2Y1 Receptor. *Sci. Rep.* (2017).

22. Shen J, DiCorleto PE. ADP stimulates human endothelial cell migration via P2Y1 nucleotide receptor-mediated mitogen-activated protein kinase pathways. *Circ. Res.* (2008).

23. Borowicz S, Van Scoyk M, Avasarala S, *et al.* The soft agar colony formation assay. *J. Vis. Exp.* (2014).

24. Pehkonen H, Lento M, Von Nandelstadh P, *et al.* Liprin-α1 modulates cancer cell signaling by transmembrane protein CD82 in adhesive membrane domains linked to cytoskeleton. *Cell Commun. Signal.* (2018).

25. Hubbard T, Barker D, Birney E, *et al.* The Ensembl genome database project. *Nucleic Acids Res.* (2002).

26. Andrews S. FASTQC A Quality Control tool for High Throughput Sequence Data. *Babraham Inst.* (2015).

27. Dobin A, Davis CA, Schlesinger F, *et al.* STAR: Ultrafast universal RNA-seq aligner. *Bioinformatics*. (2013).

28. Li H, Handsaker B, Wysoker A, *et al.* The Sequence Alignment/Map format and SAMtools. *Bioinformatics*. (2009).

29. Anders S, Pyl PT, Huber W. HTSeq-A Python framework to work with high-throughput sequencing data. *Bioinformatics*. (2015).

30. Love MI, Huber W, Anders S. Moderated estimation of fold change and dispersion for RNA-seq data with DESeq2. *Genome Biol.* (2014).

31. Benjamini Y, Hochberg Y. Controlling the false discovery rate: a practical and powerful approach to multiple testing. *J. R. Stat. Soc. Ser. B*. (1995).

32. Ashburner M, Ball CA, Blake JA, *et al.* Gene ontology: Tool for the unification of biology. Nat. Genet. (2000).

33. Yu G, Wang LG, Han Y, He QY. ClusterProfiler: An R package for comparing biological themes among gene clusters. *Omi. A J. Integr. Biol.* (2012).

34. Kanehisa M, Goto S. KEGG: Kyoto Encyclopedia of Genes and Genomes. Nucleic Acids Res. (2000).

35. Wang HY, Kim NH. CDK2 is required for the DNA damage response during porcine early embryonic development. *Biol. Reprod.* (2016).

36. Gao SY, Li J, Qu XY, Zhu N, Ji Y Bin. Downregulation of Cdk1 and CyclinB1 expression contributes to oridonin-induced cell cycle arrest at G2/M phase and growth inhibition in SGC-7901 gastric cancer cells. *Asian Pacific J. Cancer Prev.* (2014).

37. Hur W, Rhim H, Jung CK, *et al.* SOX4 overexpression regulates the p53-mediated apoptosis in hepatocellular carcinoma: Clinical implication and functional analysis in vitro. *Carcinogenesis*. (2010).

38. Urist M, Tanaka T, Poyurovsky M V., Prives C. p73 induction after DNA damage is regulated by checkpoint kinases Chk1 and Chk2. *Genes Dev.* (2004).

39. Mancini F, Pieroni L, Monteleone V, *et al.* MDM4/HIPK2/p53 cytoplasmic assembly uncovers coordinated repression of molecules with anti-apoptotic activity during early

DNA damage response. *Oncogene*. (2016).

40. Toledo F, Wahl GM. MDM2 and MDM4: p53 regulators as targets in anticancer therapy. Int. J. Biochem. Cell Biol. (2007).

41. Hussain T, Saha D, Purohit G, *et al.* Transcription regulation of CDKN1A (p21/CIP1/WAF1) by TRF2 is epigenetically controlled through the REST repressor complex. *Sci. Rep.* (2017).

42. Nag S, Qin J, Srivenugopal KS, Wang M, Zhang R. The MDM2-p53 pathway revisited. J. Biomed. Res. (2013).

43. Siednienko J, Gajanayake T, Fitzgerald KA, Moynagh P, Miggin SM. Absence of MyD88 Results in Enhanced TLR3-Dependent Phosphorylation of IRF3 and Increased IFN-β and RANTES Production. *J. Immunol.* (2011).

44. Matt S, Hofmann TG. The DNA damage-induced cell death response: a roadmap to kill cancer cells. Cell. Mol. Life Sci. (2016).

45. Das SP, Borrman T, Liu VWT, Yang SCH, Bechhoefer J, Rhind N. Replication timing is regulated by the number of MCMs loaded at origins. *Genome Res.* (2015).

46. Gordon E, Ravicz J, Liu S, Chawla S, Hall F. Cell cycle checkpoint control: The cyclin G1/Mdm2/p53 axis emerges as a strategic target for broad-spectrum cancer gene therapy - A review of molecular mechanisms for oncologists. *Mol. Clin. Oncol.* (2018).

47. Neganova I, Vilella F, Atkinson SP, *et al.* An important role for CDK2 in G1 to S checkpoint activation and DNA damage response in human embryonic stem cells. *Stem Cells*. (2011).

48. Peyressatre M, Prével C, Pellerano M, Morris MC. Targeting cyclin-dependent kinases in human cancers: From small molecules to peptide inhibitors. Cancers (Basel). (2015).

49. Haque S, Morris JC. Transforming growth factor-β: A therapeutic target for cancer. Hum. Vaccines Immunother. (2017).

50. Xu J, Lamouille S, Derynck R. TGF-B-induced epithelial to mesenchymal transition. Cell Res. (2009).

51. Ampuja M, Jokimäki R, Juuti-Uusitalo K, Rodriguez-Martinez A, Alarmo EL, Kallioniemi A. BMP4 inhibits the proliferation of breast cancer cells and induces an MMP-dependent migratory phenotype in MDA-MB-231 cells in 3D environment. *BMC Cancer*. (2013).

52. Du R, Liu B, Zhou L, *et al.* Downregulation of annexin A3 inhibits tumor metastasis and decreases drug resistance in breast cancer. *Cell Death Dis.* (2018).

53. Peitsch WK, Doerflinger Y, Fischer-Colbrie R, *et al.* Desmoglein 2 depletion leads to increased migration and upregulation of the chemoattractant secretoneurin in melanoma cells. *PLoS One*. (2014).

54. Shen H, Xu L, You C, *et al.* miR-665 is downregulated in glioma and inhibits tumor cell proliferation, migration and invasion by targeting high mobility group box 1. *Oncol. Lett.*

(2021).

55. Woodfield SE, Shi Y, Patel RH, *et al.* MDM4 inhibition: a novel therapeutic strategy to reactivate p53 in hepatoblastoma. *Sci. Rep.* (2021).

56. Fukasawa K, Vande Woude GF. Synergy between the Mos/mitogen-activated protein kinase pathway and loss of p53 function in transformation and chromosome instability. *Mol. Cell. Biol.* (1997).

57. Mor O, Yaron P, Huszar M, *et al.* Absence of p53 Mutations in Malignant Mesotheliomas. *Am. J. Respir. Cell Mol. Biol.* (1997).

58. Okuda T, Otsuka J, Sekizawa A, *et al.* p53 mutations and overexpression affect prognosis of ovarian endometrioid cancer but not clear cell cancer. *Gynecol. Oncol.* (2003).

59. Chen L, Wang S, Zhou Y, *et al.* Identification of early growth response protein 1 (EGR-1) as a novel target for JUN-induced apoptosis in multiple myeloma. *Blood*. (2010).

60. Fan M, Goodwin ME, Birrer MJ, Chambers TC. The c-Jun NH2-terminal protein kinase/AP-1 pathway is required for efficient apoptosis induced by vinblastine. *Cancer Res.* (2001).

61. Saha MN, Jiang H, Yang Y, *et al.* Targeting p53 via JNK pathway: A novel role of RITA for apoptotic signaling in multiple myeloma. *PLoS One*. (2012).

62. Chen J. The cell-cycle arrest and apoptotic functions of p53 in tumor initiation and

progression. *Cold Spring Harb. Perspect. Med.* (2016).

63. Domercq M, Brambilla L, Pilati E, Marchaland J, Volterra A, Bezzi P. P2Y1 Receptor-evoked Glutamate Exocytosis from Astrocytes. *J. Biol. Chem.* (2006).

64. Shadfan M, Lopez-Pajares V, Yuan ZM. MDM2 and MDMX: Alone and together in regulation of p53. Transl. Cancer Res. (2012).

65. Pearson AS, Spitz FR, Swisher SG, *et al.* Up-regulation of the proapoptotic mediators Bax and Bak after adenovirus-mediated p53 gene transfer in lung cancer cells. *Clin. Cancer Res.* (2000).

66. Zhu J, Chen M, Chen N, *et al.* Glycyrrhetinic acid induces G1-phase cell cycle arrest in human non-small cell lung cancer cells through endoplasmic reticulum stress pathway. *Int. J. Oncol.* (2015).

67. Higgins SP, Tang Y, Higgins CE, *et al.* TGF-β1/p53 signaling in renal fibrogenesis. Cell. Signal. (2018).

68. Oh IR, Raymundo B, Kim MJ, Kim CW. Mesenchymal stem cells co-cultured with colorectal cancer cells showed increased invasive and proliferative abilities due to its altered p53/TGF-β1 levels. *Biosci. Biotechnol. Biochem.* (2020).

69. Gen SW. The functional interactions between the p53 and MAPK signaling pathways. Cancer Biol. Ther. (2004).

70. van der Vorst EPC, Theodorou K, Wu Y, *et al.* High-Density Lipoproteins Exert Pro-inflammatory Effects on Macrophages via Passive Cholesterol Depletion and PKC-NF-κB/STAT1-IRF1 Signaling. *Cell Metab.* (2017).

71. Chen L, He HY, Li HM, *et al.* ERK1/2 and p38 pathways are required for P2Y receptor-mediated prostate cancer invasion. *Cancer Lett.* (2004).

72. Hafner A, Bulyk ML, Jambhekar A, Lahav G. The multiple mechanisms that regulate p53 activity and cell fate. Nat. Rev. Mol. Cell Biol. (2019).

73. Muscella A, Vetrugno C, Antonaci G, Cossa LG, Marsigliante S. PKC-δ/PKC-α activity balance regulates the lethal effects of cisplatin. *Biochem. Pharmacol.* (2015).

74. Basu A. Involvement of protein kinase C-δ in DNA damage-induced apoptosis. J. Cell. Mol. Med. (2003).

75. Chuderland D, Seger R. Calcium regulates ERK signaling by modulating its protein-protein interactions. *Commun. Integr. Biol.* (2008).

76. Liu Y, Song X, Shi Y, *et al.* WNK1 activates large-conductance Ca2+-activated K+ channels through modulation of ERK1/2 signaling. *J. Am. Soc. Nephrol.* (2015).